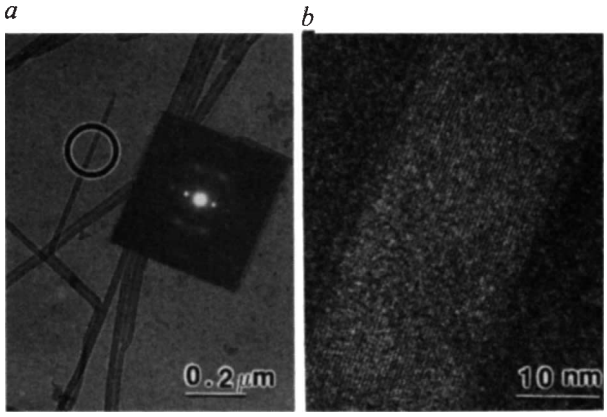

Fig. 3 *a*, As Fig. 2, but unshadowed and observed in low-dose mode. Insert: electron diffraction pattern of single whiskers. *b*, High-resolution electron micrograph, printed in reverse contrast, of a single PTFE whisker. Note the parallel lattice fringes at a spacing of 0.49 nm. The original micrograph (before photographic enlargement) was at a magnification of 46,000, an accelerating voltage of 120 kV and an accumulated electron dose of 1 electron per $Å^2$ (details in ref. 10).

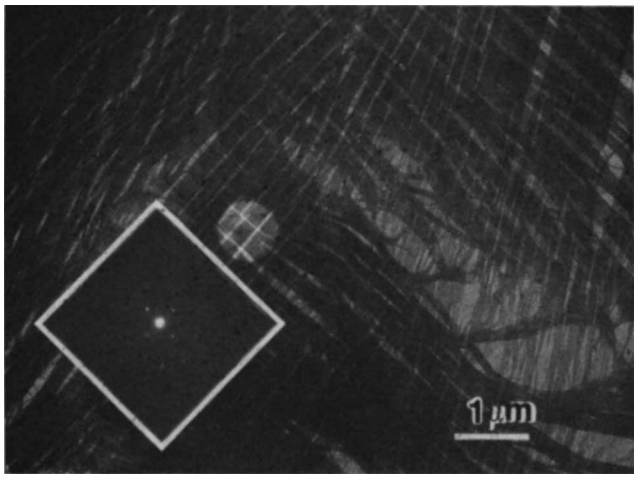

Fig. 4 Transmission electron micrograph of the dried liquid crystalline suspension of PTFE whiskers. Insert: electron diffraction of the circled area.

reveals the existence of large domains of oriented whiskers. The two domains seen in this picture are oriented roughly perpendicular with respect to one another. The insert of Fig. 4 is the electron diffractogram of the marked (bright) area. It shows a 'four point'-pattern corresponding to the two perpendicular orientations of the domains. The sharp reflections in the diffraction pattern are indicative of the local perfection of the parallel packing of the individual PTFE whiskers.

So far we have addressed the production of PTFE dispersions that showed a separation into an isotropic and an anisotropic phase. Remarkably, if the surfactant $C_8F_{17}SO_3K$ was used in the polymerization performed under otherwise identical conditions, an entirely liquid crystalline suspension was obtained. On the other hand, if either of the two above-mentioned surfactants was used at relatively low concentrations, such as 0.1% w/w, no birefringent phase was observed; at such low surfactant concentrations, only spherical PTFE particles were formed and few, if any, whiskers were found.

Although our understanding of the production of the liquid crystalline suspensions of PTFE whiskers is not complete, it is evident (see also ref. 11) that their formation is dominated by the action of the surfactant. Currently it is thought that tetrafluoroethylene in aqueous emulsion tends to polymerize and simultaneously crystallize into extended chain whiskers—primarily because the polymerization proceeds at temperatures far below the melting point of the final polymer[12]—provided that the growing particle is protected by surfactant against the very high polymer/water interfacial forces. The surfactant is also believed to prevent premature flocculation of the growing rods. Some indications now exist that the presence of surfactant in the polymerization, at a level above its critical concentration for rod-like micelle formation, is necessary for the production of the liquid crystalline suspensions. The influence of the chemical nature of the surfactant on the formation of entirely anisotropic suspensions or separated isotropic and anisotropic phases remains obscure for the time being.

The liquid crystalline suspensions described above illustrate once more that spontaneous ordering is not the exclusive property of solutions or melts of (semi-) rigid molecules. Here it is demonstrated that flexible synthetic macromolecules, when assembled into asymmetric objects such as the present extended-chain whiskers, may also exhibit the fascinating and useful (see ref. 13) self-alignment phenomenon that leads to liquid crystalline order. It is believed that this finding will provide new avenues for processing flexible macromolecules into highly ordered materials with anticipated superior performance.

We thank Dr C. R. Fincher for performing the magnetic field experiments and Drs A. D. English and H. W. Starkweather Jr for helpful comments.

Received 22 December 1987; accepted 23 March 1988

1. Onsager, L. *Ann. N.Y. Acad. Sci.* **51**, 627-659 (1949).
2. Isihara, A. *J. chem. Phys.* **18**, 1446-1449 (1950); ibid **19**, 1142-1147 (1951).
3. Flory, P. J. *Proc. R. Soc.* **A234**, 73-89 (1956).
4. Perutz, M. F., Lignori, A. M. & Eirich, S. *Nature* **167**, 929-931 (1951).
5. Bawden, F. C. & Pirie, N. W. *Proc. R. Soc.* **B123**, 274-320 (1937).
6. Marchessault, R. H. Morehead, F. F. & Walters, N. M. *Nature* **184**, 632-633 (1959).
7. *Polymer Liquid Crystals* (eds Ciferri, A., Krigbaum, W. R. & Meyer, R. B.) (Academic, New York, 1982).
8. *Liquid Crystalline Order in Polymers* (ed. Blumstein, A.) (Academic, New York, 1978).
9. Suwa, T., Takehisha, M. & Machi, S. *J. appl. Polym. Sci.* **17**, 3253-5257 (1973).
10. Chanzy, H. D., Smith, P. & Revol, J.-F. *J. Polym. Sci. Polym. Lett.* **24**, 557-564 (1986).
11. Berry, K. L. *U.S. Patent* 2,559,750 (Du Pont, 1951).
12. Wunderlich, B. *Adv. Polym. Sci.* **5**, 568-619 (1968).
13. Schaefgen, J. R. *et al.*, in *Ultra-high Modulus Polymers* (eds Ciferri, A. & Ward, I. M.) 173-201 (Applied Science, London, 1979).

The dispersal of the Amazon's water

Frank E. Muller-Karger*, Charles R. McClain† & Philip L. Richardson‡

* Horn Point Environmental Laboratories, University of Maryland, Box 755, Cambridge, Maryland 21613, USA
† NASA, Goddard Space Flight Center, Greenbelt, Maryland 20771, USA
‡ Woods Hole Oceanographic Institution, Woods Hole, Massachusetts 02543, USA

The Amazon is the largest river system in the world, contributing about 6×10^{12} m^3 of fresh water to the tropical Atlantic each year[1,2]. This is about 16% of the annual discharge into the world's oceans. Yet the fate of this water and of the dissolved and particulate material discharged with it[3,4] has remained unclear. Previous observations of 300-km diameter lenses of Amazon water off South America[2,5] and a plume that extends into the Atlantic[6,7] indicate some offshore movement, but the relationship of these and alongshore currents has remained obscure. New information, obtained with NASA's Coastal Zone Color Scanner (CZCS) and with drifting buoys, reveals that the discharge of the Amazon is carried offshore around a retroflection of the North Brazil Current and into the North Equatorial Countercurrent towards Africa between June and January each year. From about February to May the countercurrent and the retroflection weaken or vanish, and Amazon water flows northwestward towards the Caribbean Sea.

We studied the dispersal of Amazon water with 32 CZCS satellite images collected between November 1978 and December 1982, and with trajectories of surface drifters released from ships between 1983 and 1986. Visible radiance backscattered out of the upper optical depth of the ocean was estimated from the CZCS radiance[8-10]. Pigment concentrations (chlorophyll *a* plus phaeopigments and dissolved organic material) were estimated from the water-leaving radiance by using empirical relationships based on ratios of the blue or blue-green (443 or 520 nm) relative to the green (550 nm)[8-10] radiances. Previous studies have shown that in relatively clear oceanic water, pigment estimates are within 30-40% of average near-surface phytoplankton pigment concentrations[9,11]. Nearshore, pigment concentrations are less reliable and were considered only qualitatively. Inshore of the 10 m isobath directly off the Amazon delta, high pigment concentrations (>5 mg m^{-3}; Figure 1) reflect turbidity due to suspended sediment[4]. A permanent phytoplankton bloom occurs between the 10 and 30 m isobaths (pigment up to 30 mg m^{-3}; P. Dustan personal communication), where suspended sediments in surface waters decrease to <10 mg sediment per liter[4], allowing light to penetrate deeper. Currents off the delta advect this water and an abundant flora of neritic diatoms[12] northwestward along the coast of Brazil.

A comparison of the CZCS images and tracks of surface-drifting objects[13] north of the Amazon delta provided a consistent picture of a fairly regular seasonal cycle. The path followed by the Amazon water during February-May was different from that traced during June-January (Fig. 1). During February-May, Amazon water flowed into the Caribbean in a broad (150-200 km), continuous band of high concentrations of pigment (>1.5 mg m^{-3}) and sediment (Fig. 1, *Top*). Offshore, a large area in the tropical Atlantic contained pigment concentrations >0.2 mg m^{-3}, compared with the <0.15 mg m^{-3} background concentrations in oceanic water. This is a result of earlier offshore movement of shelf water during June-January. During February-May, surface drifters in the tropical Atlantic moved westward until they were within a few hundred km of the coast, where they turned and drifted more northwestward. The trajectories implied a continuous boundary current with characteristic speeds of ~ 90 cm s^{-1}.

During June-January, five buoys veered offshore near 5° N 50° W and continued eastward, following a meandering pattern (Fig. 1, *Bottom*). This retroflection of the North Brazil Current (NBC) is the western source of the North Equatorial Countercurrent (NECC). A similar pattern was observed in the June-January CZCS images, indicating that Amazon water was being carried offshore around the retroflection and into the NECC. Pigment concentrations in the plume were highest near the continental margin (>1.5 mg m^{-3}) and decreased to about 0.4 mg m^{-3} 1,000 km into the NECC. The patterns seen during June-January were similar to the distribution of sea-surface salinity (Fig. 2), and agreed with historical ship drifts[14] and numerical models[15]. The continuity in the distribution of pigments showed the Amazonian origin of the offshore plume and is evidence that the whole near-surface NBC retroflects.

The shape of the retroflection seems to be due to an overshoot by the NBC past the mean latitude of the NECC (8° N), followed by a quasistationary wave train downstream (Figs 1 and 3) The images revealed that the northern crest of the retroflection frequently reached 11° N, 53° W, and that a southern meander trough formed near 4.5° N, 46° W. A second oscillation was evident with a trough near 4.5° N, 39° W. The average wavelength of the meanders was 730 km. The centre of the retroflection was near 8° N, 51° W, where a depression in the thermocline has been observed repeatedly[16].

From August to October, buoys in the NBC drifted past the Amazon mouth at speeds of about 90 cm s^{-1} and then retroflected, reaching 45° W in about 18 days. From here they gradually slowed to 30 cm s^{-1} as they drifted eastward. About half the buoys in the NECC continued eastward into the Guinea Current near Africa. The other half moved northward into the North Equatorial Current (NEC) and then westward.

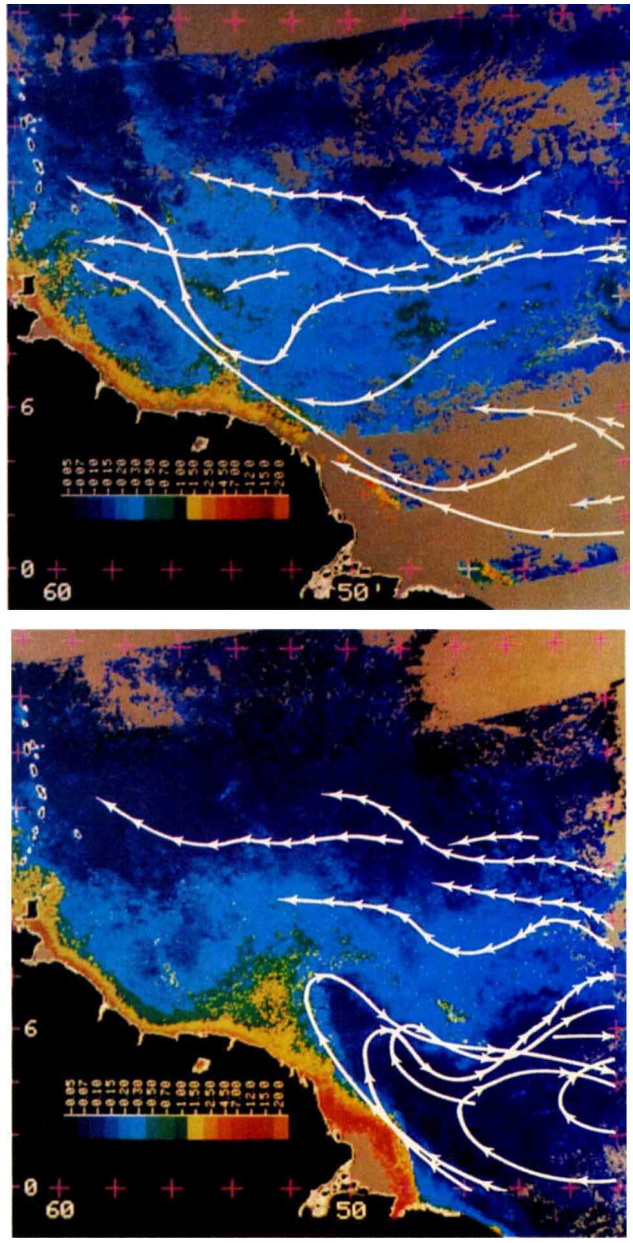

Fig. 1 Seasonal composites of CZCS images and surface drifters for the western tropical Atlantic. The CZCS composites show the mean pigment value [mg m^{-3}] of cloud-free pixels in sets of images collected during 1979-80. Land was masked black and clouds or missing data grey. Smoothened trajectories of buoys tracked from 1983 to 1986 (ref. 13) were added to the composites. Arrowheads are spaced at five-day intervals. Some trajectories were omitted to reduce clutter. *Top*, a composite of five images from 15 January to 20 February 1980 and trajectories for January-June. The Amazon plume appears as a wide yellow-orange band along the coast. Offshore, the blue-green colours indicate the region over which Amazon water from the previous season is dispersed. *Bottom*, a composite of 15 images from 21 July 1979 to 9 January 1980 and trajectories for July-December. The plume is carried offshore near 6-8° N as seen by yellow and green values fading to light blue in contrast to dark blue oceanic water.

These circulation patterns indicate that Amazon water discharged during June-January (about 60% of the annual discharge) may take between a few months and a year to reach

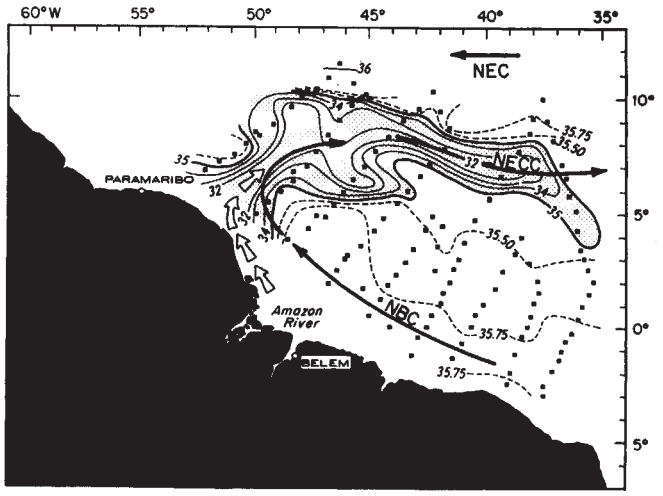

Fig. 2 Quasi-synoptic map of sea-surface salinity for the period 24 July to 11 September 1964 (ref. 7). Arrows were added to show the inferred path of low-salinity Amazon water and major currents.

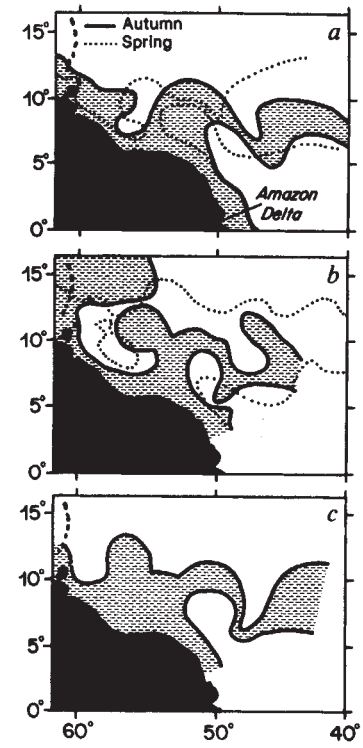

Fig. 3 Schematic representation of the Amazon plume as observed in seasonal composites of CZCS images for (*a*) 1979, *b*, 1980 and *c*, 1981. No images were available for February–May 1981. Pigment contours follow approximately the 0.3 mg m^{-3} isopleth and were smoothened for clarity. Stippled areas represent the June–January (northern autumn) extent of the plume, broken lines show February–May conditions (northern spring).

the Caribbean. Also, while the discharge of one year drifts westward in the NEC, water entrained in a newly formed NECC may mix with some of the older discharge. A fraction of Amazon water may continue moving eastward and reach Africa, as indicated in a global composite of CZCS imagery for December 1981 (G. C. Feldman, personal communication).

The patterns of plume dispersal vary from year to year (Fig. 3). For example, during February–May of 1979, the retroflection elongated to the northeast as seen in a CZCS composite of May 1979[17]. Also, during June–January of 1980 and 1981, some Amazon water was lost to the northwest, away from that retroflecting into the NECC (Fig. 3). Spatial variability is so large in this region that coarse sampling from ships could lead to misconceptions about the circulation.

This information is conclusive evidence that the low salinity (34.8–35.0‰) observed across the tropical Atlantic between 5° and 10° N (ref. 18) is not solely due to precipitation associated with the Intertropical Convergence Zone (ITCZ)[19]. But the processes that lead to the formation of the retroflection of the NBC and the offshore transport of Amazon water are not clear. Numerical models indicate that the NECC forms owing to variation in the curl of the wind stress associated with the ITCZ and geostrophic adjustment of the water[15,20]. In addition, the NBC, which has negligible planetary vorticity near the Equator, flows into a region of waters with positive vorticity[21]. This combination of factors may cause the pronounced anticyclonic turn of the NBC. Similar processes may be reponsible for the seasonal eastward turn of the Somali Current[22].

The patterns described above help explain the variability of salinity and pigments observed at Barbados[23]. Also, the greater flux of organic particulates to the bottom of the tropical Atlantic relative to the tropical central Pacific[24] may be explained if the Amazon plume contains abundant phytoplankton. But it is still not clear how such large amounts of phytoplankton could remain viable in the plume. There are several likely sources of nutrients for phytoplankton. Upwelling takes place inshore of the retroflection[5,25,26] and also possibly along crests in the NECC, where geostrophic adjustment occurs. Recycling of nutrients within the plume probably plays a major role, and grazing by zooplankton, sinking, and mixing with nutrient-poor oceanic water limit the horizontal extent of the blooms. None of these variables has been studied yet.

The many different paths taken by Amazon water depend on the variability of the retroflection and of the NECC. Owing to the large scale of the processes observed, future studies in the western tropical Atlantic need to be mutidisciplinary and done from platforms that provide synoptic information. Such studies need to address plankton dynamics to arrive at a better understanding of the geochemical effects of the Amazon River on the interior Atlantic Ocean.

We thank John Sissala, Mike Doline and Richard Sipes (Nimbus Operations, General Electric) for their help in selecting the imagery; Judy Chen, Mike Darzi and Jim Firestone (General Sciences Corporation) for implementing the image-processing system (SEAPAK); and Tom Fisher and Bill Schmitz for helpful comments on the manuscript. This work was supported by the NASA Graduate Student Researcher's Program, the Ocean Processes Branch of NASA Headquarters, and the National Science Foundation.

Received 16 November 1987; accepted 29 February 1988.

1. Sioli, H. in *River Ecology* (ed. Wretton, B. A.) 461–488 (Blackwell, London, 1975).
2. Gibbs, R. J. *J. mar. Res.* **28**, 113–132 (1970).
3. Milliman, J. D. & Meade, R. H. *J. Geol.* **91**, 1–21 (1983).
4. Nittrouer, C. A., Curtin, T. B. & DeMaster, D. J. *Cont. Shelf Res.* **6**, 151–174 (1986).
5. Ryther, J. H., Menzel, D. W. & Corwin, N. *J. mar. Res.* **25**, 69–83 (1967).
6. Perlroth, I. in *Proc. Symp. Oceanogr. Fisheries Resources trop. Atlantic* 185–191 (UNESCO, Paris, 1966).
7. Cochrane, J. D. *J. mat. Res.* **27**, 327–334 (1969).
8. Clark, D. K. in *Oceanography from Space* (ed. Gower, J. F. R.) 227–237 (Plenum, New York, 1981).
9. Gordon, H. R. *et al. Appl. Opt.* **22**, 20–36 (1983).
10. Gordon, H. R. *et al. Appl. Opt.* **22**, 3929–3931 (1983).
11. Gordon, H. R. *et al. J. mar. Res.* **40**, 491–502 (1982).
12. Wood, E. J. *Bull. mar. Sci.* **16**, 102–123 (1966).
13. Richardson, P. L. & Reverdin, G. *J. geophys. Res.* **92**, 3691–3708 (1987).
14. Richardson, P. L. & Walsh, D. *J. geophys. Res.* **91**, 10537–10550 (1986).
15. Philander, S. G. H. & Pacanowski, R. C. *J. geophys. Res.* **91**, 14192–14206 (1986).
16. Bruce, J. G., Kerling, J. L. & Beatty, W. H. III *Prog. Oceanogr.* **14**, 57–63 (1985).
17. Esaias, W. E., Feldman, G. C., McClain, C. R. & Elrod, J. A. *Eos* **67**, 835–837 (1986).

18. Henin, C., Hisard, P. & Piton, B. *FOCAL* Vol 1 (ORSTOM, Paris, 1986).
19. Neumann, G. *Deep Sea Res.* Suppl **16**, 165-177 (1969).
20. Busalacchi, A. J. & Picaut, J. *J. phys. Oceanogr.* **13**, 1564-1588 (1983).
21. Csanady, G. T. *J. mar. Res.* **43**, 553-579 (1985).
22. Bruce, J. G. *J. phys. Oceanogr.* **14**, 826-832 (1984).
23. Borstad, G. A. *J. mar. Res.* **40**, 421-434; 435-452 (1982).
24. Pilskaln, C. H. & Honjo, S. *Global biogeochem. Cycles* **1**, 31-48 (1987).
25. Mazeika, P. A. *Dt. hydrogr. Z.* **26**, 49-73 (1973).
26. Gibbs, R. J. *Deep Sea Res.* **A27**, 857-866 (1980).

D/H ratios of environmental water recorded by D/H ratios of plant lipids

Leonel da Silveira Lobo Sternberg

Department of Biology, University of Miami, Coral Gables, Florida 33124, USA

Isotope ratios of chemical components are powerful tools in the interpretation of palaeoenvironments, particularly carbonates from foraminiferans[1,2], desert caliche[3], and desert pavements[4]. Isotope ratios of plant cellulose are also indicators of environmental variables such as temperature and relative humidity[5-7]. Several workers have reported climatic fluctuations based on hydrogen and oxygen isotope ratios of cellulose from tree trunks[8-10] and peats[11,12]. Here I present measurements that demonstrate that for submerged aquatic plants δD values of lipids record D/H ratios of environmental water, whereas cellulose does not. I further demonstrate that δD values of lipids in conjunction with δ^{18}O values of cellulose provide significant information on isotope ratios of environmental water.

Oxygen and hydrogen isotope ratios of plant cellulose were first proposed as palaeoclimatic indicators because isotope ratios of rainwater (meteoric water as defined by Craig[13]) are related to climate; that is, rainwater from warmer regions at lower latitudes or altitudes has high D/H and $^{18}O/^{16}O$ ratios, whereas in cooler regions at higher latitudes or altitudes these ratios are lower. Plants record the hydrogen and oxygen isotope ratios of water available for growth in their cellulose[5-7]. Thus deducing climate through isotope ratios of meteoric water is a matter of deciphering the isotopic fractionations that take place during water uptake, evapotranspiration and incorporation into cellulose. The major problems with the use of cellulose to interpret climate, however, are the effect of evapotranspiration in modifying isotopic ratios of leaf water relative to ground water[7,14], and species-specific variable isotopic fractionations that occur during metabolic processes responsible for incorporation of hydrogen in cellulose[15-20]. Particularly relevant to this paper is the latter problem. Large variability in δD values of non-exchangeable hydrogens from cellulose of different species of plants grown in a single site, exposed to the same climate and meteoric water, have been observed[15,16]. This variability also extends to aquatic plants, indicating that variable hydrogen isotopic fractionations during cellulose synthesis are primarily due to fractionations occurring during biochemical reactions[17,18]. In addition, fractionations occurring during biochemical reactions are influenced by environmental factors such as temperature[19] and light quality[20]. As a result of this variability, absolute δD values of water available during cellulose synthesis cannot be deduced from hydrogen isotope ratios of cellulose. Differences in hydrogen isotope ratios of plant cellulose through time can be due to changes in δD values of groundwater, to differences in isotopic fractionations particular to each species, or to environmental effects on the hydrogen isotope fractionations occurring during cellulose synthesis. Thus climatic information from hydrogen isotope ratios of cellulose cannot be precisely estimated.

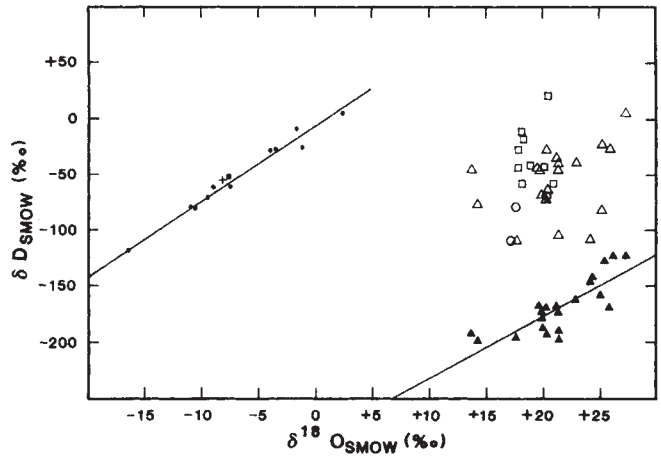

Fig. 1 The relationship between δD and δ^{18}O values of lake waters, δD values of non-exchangeable hydrogen of cellulose and δ^{18}O values of cellulose from submerged aquatic plants, and δD values of lipids and δ^{18}O values of cellulose. Symbols: ●, isotope ratios of lake water in this study; +, ■, isotope ratios of waters measured by DeNiro and Epstein[19] and Epstein *et al.*[5] respectively; △, isotope ratios of cellulose measured in this study; □, ○, isotope ratios of cellulose measured by DeNiro and Epstein[19] and Epstein *et al.*[5] respectively; ▲, δD values of lipids versus δ^{18}O values of cellulose. Correlation coefficients, *r*, were 0.95 for water values, 0.38 for cellulose values, and 0.80 for lipids versus cellulose values.

There are three possible solutions to this problem. The first and most difficult is a complete understanding of all isotopic fractionations occurring during water uptake through cellulose synthesis for different species. This knowledge can then be used to deduce δD values in meteoric water from isotope ratios of plant cellulose. The second is to find a single species whose isotopic fractionations do not vary between individuals of the same species or with environmental conditions. The third solution, specifically addressed here, is the analysis of a plant component that incorporates deuterium without the metabolic effects observed for cellulose. Previous D/H ratio measurements in lipids and cellulose from plants show that whereas cellulose has a large variation in δD relative to the δD of the available water, lipids have a relatively constant δD value[21,22]. Thus lipids may be a plant metabolic component that truly records the δD values of environmental waters.

The feasibility of using δD values of lipids in conjunction with δ^{18}O values of cellulose to deduce isotope ratios of meteoric water is demonstrated here. Submerged aquatic plants from several lakes of different geographical regions having water with different isotope ratios were collected and $^{18}O/^{16}O$ and/or D/H ratios of their cellulose and lipids, and the surrounding water, were determined (Table 1). Submerged aquatic plants are ideal organisms for this analysis because they do not transpire, and transpiration modifies the isotope ratio of water available for cellulose synthesis relative to the water source[14]. δD and δ^{18}O values of lake waters were highly correlated with each other ($r = 0.95$, $P < 0.01$, Fig. 1) and this relation is expressed by the regression equation

$$\delta D_{water} = 6.7\delta^{18}O_{water} - 6.9 \quad (1)$$

The slope of this regression line (6.7) is smaller than that of meteoric water (8.0) (ref. 13). As lakes of warmer regions at lower altitudes evaporate more rapidly, they may have a disproportionate increase in δ^{18}O values of the water relative to increases in δD values due to kinetic effects, thus decreasing the slope of the line. δD values of extracted and nitrated plant cellulose were not related to the δD values of lake water